Front. Earth Sci. 2022, 16(2): 304–322
https://doi.org/10.1007/s11707-021-0890-0

RESEARCH ARTICLE

Sensitivity of Typhoon Lingling (2019) simulations to horizontal mixing length and planetary boundary layer parameterizations

Siqi CHEN[1,2], Feng XU[1,2], Yu ZHANG (✉)[1,2,3], Guiling YE[1,2], Jianjun XU[1,2,3], Chunlei LIU[1,2,3]

1 College of Ocean and Meteorology, Guangdong Ocean University, Zhanjiang 524088, China
2 South China Sea Institute of Marine Meteorology, Zhanjiang 524088, China
3 Shenzhen Institute of Guangdong Ocean University, Shenzhen 518120, China

Abstract Forecasting the intensity of typhoons is a difficult problem in numerical weather prediction. It is subject to many factors, among which the selection of physical parameterization schemes for the model is a hot topic of research. In this study, the effects of horizontal mixing length (represented by *h_diff*) and planetary boundary layer (PBL) schemes were investigated. Six idealized and four operational sensitivity experiments were designed based on simulation of the typhoon Lingling, which occurred over the western Pacific in 2019, using the Hurricane Weather Research and Forecasting model. The results of the idealized experiments showed that, as *h_diff* was increased, the slope of the typhoon eye area also increased, and its intensity became stronger. On the other hand, the results of the sensitivity experiments indicated that the intensity of the simulated typhoon was sensitive to the choice of PBL scheme, with the forecast bias of the QNSE (Quasi-Normal Scale Elimination) scheme being smaller than that of the GFDL (Geophysical Fluid Dynamics Laboratory) scheme. Angular momentum budget analyses indicated that, when increasing the *h_diff*, the convergence of angular momentum was larger in the boundary layer, which led to a faster spin-up of the vortex, further increasing the intensity of the typhoon. From the calculated horizontal and vertical vortex spread it was found that, when the *h_diff* was increased, the corresponding horizontal and vertical diffusion eddies also showed an increasing trend, which was also the reason for the strengthening of the typhoon. Meanwhile, the forecast bias decreased significantly with increasing horizontal mixing length when using the same PBL scheme.

Keywords Hurricane Weather Research and Forecasting model, planetary boundary layer, western Pacific, typhoon, horizontal diffusion

Received October 25, 2020; accepted March 15, 2021

E-mail: zhangyu2@gdou.edu.cn

1 Introduction

With the development of numerical weather prediction models, typhoon track forecasts have been significantly improved, but intensity forecasts still show large errors (Xue et al., 2013), especially for explosive typhoons. The forecasting uncertainty is closely associated with the choice of boundary layer parameterization scheme. In particular, the transmission of heat, momentum and turbulence at the air–sea interface near the typhoon eyewall region plays a vital role in typhoon forecasting (Emanuel, 1995; Persing and Montgomery, 2003; Rotunno et al., 2009). Tang et al. (2018b) conducted two sensitivity experiments using different planetary boundary layer (PBL) schemes and found that the storm intensity in the boundary layer was stronger in the MYJ (Mellor–Yamada–Janjic) scheme run than in the Geophysical Fluid Dynamics Laboratory (GFDL) scheme run. Tropical cyclones (TCs) are strongly sensitive to the choice of PBL scheme, including the parameterization of turbulent momentum fluxes and moist enthalpy across the air–sea interface (Nolan et al., 2009; Braun and Tao, 2000; Green and Zhang, 2014). In the boundary layer parameterization scheme, the boundary layer height also has an important influence on simulation of the typhoon intensity. Ma et al. (2018) conducted related sensitivity experiments and found that unbalanced dynamics due to varying the boundary layer height were more pronounced and contributed to a more rapidly intensifying TC. Rajeswari et al. (2020) carried out 25 sensitivity experiments and showed that the physics of the Quasi-Normal Scale Elimination (QNSE) scheme mainly affected the intensity. The stronger inflow, spin-up and stronger wind-induced transport of energy fluxes in the QNSE scheme led to stronger convection and a higher intensification of TCs in these simulations.

Hariprasad et al. (2014) conducted sensitivity experiments using seven PBL schemes and their results indicated

that the QNSE scheme produced highly unstable and deep convective layers and higher eddy diffusivities over the unstable regime than that over the stable regime. Horizontal diffusion associated with the PBL and turbulent processes in typhoon forecasts have been paid a considerable amount of attention in previous studies (Emanuel, 1997; Bryan, 2012; Zhang and Marks, 2015). Theoretical and numerical studies have indicated that turbulent processes in the PBL play an essential role in the maintenance and intensification of hurricanes (Ooyama, 1969; Smith et al., 2009). Malkus and Riehl (1960) proposed for the first time that the surface heat and momentum exchange coefficient of the maximum tangential wind are factors that affect the development of typhoons. It has been found that the increase in sensible and latent heat in a single-layer boundary layer scheme will lead to a stronger hurricane (Ooyama, 1969; Rosenthal, 1971; Emanuel, 1986). Simulations that only change the surface flux show that the intensity of the simulated hurricane increases as the ratio of enthalpy and momentum exchange coefficient (C_k/C_d) increases. Bryan (2012) changed the surface exchange coefficients (C_h/C_d) and the length scales of the horizontal diffusion in the idealized framework of the Hurricane Weather Research and Forecasting (HWRF) model and confirmed that the maximum wind speed was strongly affected by the horizontal diffusion, but the ratio of surface exchange coefficients (C_h/C_d) had less of an effect on the maximum wind speed. Rotunno and Bryan (2012) pointed out that the horizontal diffusion coefficient is the main contributor to the simulated maximum hurricane intensity, and the maximum wind depends mainly on horizontal diffusion. Zhang and Montgomery (2012) studied the characteristics of turbulent processes in rapidly intensifying hurricanes and found that the horizontal mixing length, influenced by *h_diff*, and DHD (dynamic horizontal diffusion) increased slightly with wind speed, leading to significant improvements of the boundary layer physics in the operational HWRF model (Zhang and Uhlhorn, 2012).

When the HWRF model predicts typhoons, although the effect of the boundary layer parameterization scheme on the prediction has gradually improved in the eastern Pacific basin and the western Atlantic basin (regions where the model has been put into operation), due to the western Pacific basin having different topographical conditions, there is still room here to research and improve the boundary layer parameterization scheme, plus, the configuration of the horizontal diffusion coefficient corresponding to different boundary layer parameterization schemes still needs to be further studied. The research reported in this paper was based on the 15th typhoon in 2019 (named 'Lingling'), which we simulated using idealized HWRF framework experiments and operational model experiments. The results were used to analyze the forecasting skill for typhoons in the western Pacific basin from the perspectives of dynamics and thermodynamics.

The remainder of the paper is organized into four sections, as follows: The configuration of the HWRF model and the design of the experiments are introduced in Section 2, as well as the formula for the horizontal diffusion coefficient. The results of the idealized HWRF experiments are presented in Section 3, including an evaluation of the effect of different horizontal diffusion coefficients on the typhoon structure and strength. The results from verification experiments for the HWRF idealized model are discussed in Section 4. Finally, a discussion and our conclusions are presented in Section 5.

2 Configuration and experimental design

2.1 Forecast model

The HWRF model is developed by the National Oceanic and Atmospheric Administration of the United States. The triple-nested version of HWRF-V4.0a (Biswas et al., 2018) was employed in this study. The HWRF model can be used as an atmosphere–ocean coupled model, with an atmospheric component that employs the Non-hydrostatic Mesoscale Model dynamic core of the Weather Research and Forecasting model. For the ocean part, HWRF employs the Message Passaging Interface to run a parallel version of the Princeton Ocean Model (POM) for Tropical Cyclones, which was developed at Princeton University, in the Northwest Pacific basins. Figure 1 shows the model domain used in the HWRF model. The parent domain covered roughly 77.2° × 77.2° on a rotated latitude/longitude E-staggered grid; the middle domain of about 17.8° × 17.8° moved along with the storm using two-way interactive nesting; and the inner domain of about 5.9° × 5.9° also moved along with the storm. The stationary parent domain had a grid spacing of 13.5 km, while the middle and inner grid spacing were 4.5 km and 1.5 km, respectively. The physical parameterizations used in this study are given in Table 1.

In the idealized HWRF model, the triple-nested domain configuration of the operational HWRF model was used, with the grid spacing at 13.5, 4.5, and 1.5 km, respectively. The model physics options used in this study were configured as close as possible to the operational HWRF model, which is initialized by solving the nonlinear balance equation in the pressure-based sigma coordinate system on an *f*-plane centered at 15°N (Wang, 1995). The initial axisymmetric cyclonic vortex had a maximum wind speed of 20 m/s and a radius of maximum wind speed of about 90 km embedded in a quiescent flow. The environmental temperature and humidity fields in all of the experiments were from Jordan's Caribbean sounding (Gray et al., 1975).

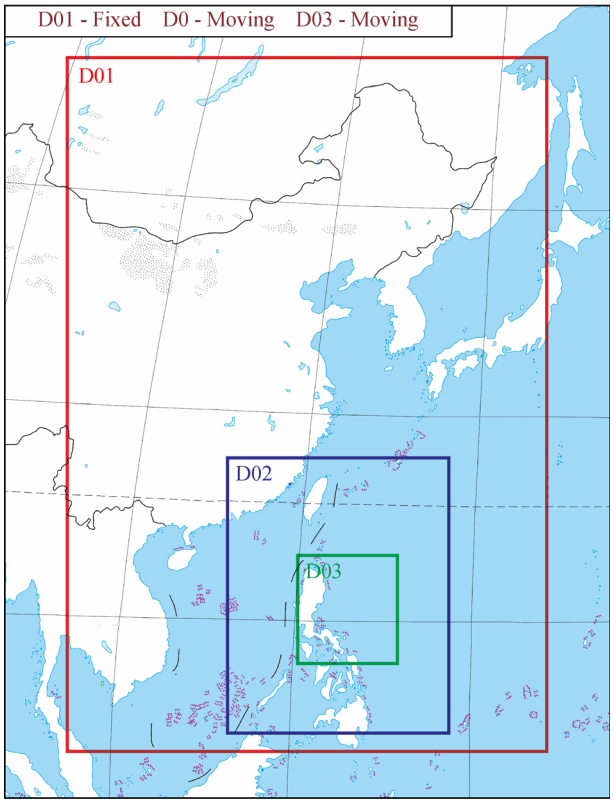

Fig. 1 The HWRF simulation domain. The red rectangle represents the domain of the fixed area (5°–55°N, 100°–140°E), and the blue and black rectangles represents the moving domain.

Table 1 Configuration of the physical parameterizations used in HWRF-v4.0a in this study

Model domain	Domain 1 : 13.5 km; Domain 2: 4.5 km; Domain 3: 1.5 km
Dynamics	Primitive equation, non-hydrostatic
Vertical resolution	75 levels
Domain	Domain 1 : 100°E–140°E, 5°N–55°N Domains 2, 3 : moving (not fixed)
Longwave radiation	Dudhia
Shortwave radiation	RRTM scheme
Cumulus convection	Simplified Arakawa–Schubert
Microphysics	Ferrier
Surface processes	GFDL
Vortex tracking algorithm	NCEP vortex tracker

2.2 Data and sources

In the operational and idealized HWRF model, both the initial and boundary conditions were taken from the NCEP's Global Forecast System (GFS) (National Centers for Environmental Prediction/National Weather Service/NOAA/U.S. Department of Commerce, 2015) analysis generated by the global ensemble-based hybrid data assimilation system. The 126-h forecasts were obtained directly from the spectral coefficients at T574L64 resolution (about 27 km near the equator and 64 vertical levels), and the boundary conditions were updated at 6-h intervals. For the GSI (Gridpoint Statistical Interpolation) assimilation system, the satellite data used in the assimilation were from GFS satellite data.

For the verification, MERRA2 (Modern-Era Retrospective Analysis for Research and Applications, Version 2) data provided by NASA (Gelaro et al., 2017) were used. For typhoon observations, the best-track dataset provided by IBTrACS was used (Knapp et al., 2010).

2.3 Experimental design

2.3.1 PBL parameterization schemes

The PBL parameterization scheme determines how energy fluxes influence the evolution of the atmosphere. It affects the exchange of vertical heat and momentum at the air-sea interface. The exchange expression is

$$\frac{\partial \overline{c}}{\partial t} = \ldots - \frac{\partial}{\partial x_j}\left(\overline{c' u_j'}\right), \tag{1}$$

where $\overline{c}$ represents meteorological elements (u,v,e,q), the horizontal line on the letter represents the average. $\overline{c' u_j'}$ controls the local variation in vertical flux and can be expressed as

$$\overline{c' u_j'} = -K_m \frac{\partial}{\partial x_j}(\overline{c}), \tag{2}$$

where K_m is the vertical vortex diffusion coefficient controlled by the following parameters:

$$K_m = Fle^{\frac{1}{2}}. \tag{3}$$

Here, F is the stability function, l is the turbulent mixing length, and e is the turbulent kinetic energy (TKE).

In HWRF-V4.0a, the PBL parameterization scheme uses the non-local Hybrid Eddy Diffusivity Mass Flux, and K_m is expressed by

$$K_m = \hat{e}Z\left(\frac{u^*}{F}\right)\left[\acute{a}\left(1-\frac{z}{h}\right)^2\right], \tag{4}$$

where $\hat{e}(0.4)$ is the von Karman Constant, u^* is the surface friction speed, F is the stability function , h is the boundary layer height, and á controls the boundary layer vortex diffusion. Because the PBL parameterization scheme is based on a K-profile method, which is not a TKE-type scheme, the term related to TKE is set to a very small value (Zhang et al., 2018) that is close to zero and is thus not shown in Eq. (4).

However, the QNSE parameterization scheme mainly focuses on the TKE, and operates with the inverse values of the stability functions. The main differences between the QNSE and GFDL schemes are shown in Table 2.

Table 2 The GFDL and QNSE PBL functions

	GFDL	QNSE
S	$\left(\frac{u_*}{F}\right)$	$S_{m,n}(Ri_{loc})$
l	á$\left(1-\frac{z}{h}\right)^2$	If $N^2 \geqslant 0$, $l=\frac{1}{l_b^{-1}+l_s^{-1}}$ where $l_b=\frac{kz}{1+\frac{kz}{\mathrm{e}}}$, $l_s=\frac{0.75\sqrt{\mathrm{TKE}}}{N}$ and ë$=\frac{0.0063u_*}{f}$ If $N^2<0$, l adjusted to satisfy an equation for $l/q,q=(2\mathrm{TKE})^{0.5}$
TKE	based on a K-profile method, TKE is set to a very small value	$\mathrm{TKE}=\mathrm{TKE}\left[l,K_M\left(\frac{\partial V}{\partial z}\right)^2,K_H N^2\right]$

2.3.2 Horizontal mixing length

For horizontal diffusion, the HWRF model uses a first-order nonlinear Smagorinsky-type parameterization (Janjić, 1990). The horizontal turbulent momentum flux F_h is controlled by the eddy diffusivity K_h,

$$F_h = \tilde{\mathrm{n}} K_h S_h, \tag{5}$$

where S_h is the horizontal strain rate of the mean flow (Stevens et al., 1999), defined as

$$S_h = \left(\frac{\partial v}{\partial x}+\frac{\partial u}{\partial y}\right). \tag{6}$$

The horizontal eddy diffusivity K_h is flow dependent:

$$K_h = L_h^2 D_h, \tag{7}$$

where L_h is the horizontal mixing length and D_h is defined as

$$D_h^2 = \left(\frac{\partial v}{\partial x}+\frac{\partial u}{\partial y}\right)^2+\left(\frac{\partial u}{\partial x}-\frac{\partial v}{\partial y}\right)^2. \tag{8}$$

The horizontal eddy diffusivities (Zhang and Marks, 2015) for heat (K_t) and moisture (K_q) are set to equal that for momentum (i.e., $K_t = K_q = K_h$) in HWRF. Note that L_h is a function of both *coac* and horizontal spacing *dx* in HWRF, in the form of $L_h^2 = coac\ dx^2$. There is also a parameter in HWRF-V4.0a, *h_diff*, which we can modify to vary the horizontal diffusion coefficient. Therefore, based on the HWRF-V4.0a operational/idealized model, this study conducted six idealized experiments (Table 2) by changing the value of *h_diff* to explore its influences on the predicted typhoon intensity.

2.3.3 Air–sea exchange coefficient

The HWRF-V4.0a model uses the bulk aerodynamic formulae to calculate surface fluxes of heat and momentum. According to the model's scientific documentation, the surface-layer schemes calculate friction velocities and exchange coefficients that enable the calculation of surface heat, moisture, and momentum fluxes by the land-sea mask (Biswas et al., 2018). In this paper, the effects of the surface exchange coefficient (C_d and C_h) and corresponding surface roughness length (z_0 and z_T) on the typhoon are investigated.

In this formulation, the neutral drag coefficient C_d is defined as

$$C_d = \hat{\mathrm{e}}^2\left(\ln\frac{Z_m}{Z_0}\right)^{-2}, \tag{9}$$

where ê is the von Karman constant (= 0.4), z_0 is the roughness length for momentum, and z_m is the lowest model-level height.

The neutral heat and humidity coefficients (assumed equal, C_h) are expressed as

$$C_h = \hat{\mathrm{e}}^2\left(\ln\frac{Z_m}{Z_0}\right)^{-1}\left(\ln\frac{Z_m}{Z_T}\right)^{-1}, \tag{10}$$

where Z_T is the roughness length for heat and humidity.

Based on idealized experiments, four operational experiments were designed (Table 3). EXPR1 and EXPR3 involved running simulations using the GFDL boundary layer parameterization scheme, but with the horizontal diffusion coefficient of EXPR1 set to 1 and that of EXPR3 set to 2. EXPR2 and EXPR4, meanwhile, involved running simulations using the QNSE boundary layer parameterization scheme, but in EXPR2 the horizontal diffusion coefficient was set to 1 and in EXPR4 it was 2. The experiments were designed to answer the following two questions: 1) between the HWRF boundary layer parameterization schemes, GDFL and QNSE, which prediction is better? 2) Based on the same boundary layer parameterization scheme for typhoon prediction, what are the different values of *h_diff*? The aims in addressing these questions were to provide useful evidence for future research on typhoon energy in the western Pacific, establishing relevant parameterization schemes more reasonably, and making better preparations for forecasting typhoons and reducing damage caused by typhoons.

3 Results

3.1 HWRF-idealized experiments using different *h_diff* values

Figure 2 shows histograms of (a) the minimum sea surface

Table 3 Experimental design for HWRF (idealized/operational)

HWRF-idealized		HWRF- operational		
	h_diff	PBL parameterization schemes		*h_diff*
IDE1	0.4	EXPR1	HWRF-GFDL	1
IDE2	0.6			
IDE3	0.8	EXPR2	HWRF-QNSE	1
IDE4	1.4			
IDE5	1.8	EXPR3	HWRF-GFDL	2
IDE6	2			
		EXPR4	HWRF-QNSE	2

pressure and (b) the maximum wind speed over 60–78 h. IDE1–IDE6 are the HWRF idealized experiments with different *h_diff* and the black histograms represent the results of IBTrACS. It can be seen that the minimum pressure and the maximum wind speed of the typhoon are very sensitive to the *h_diff* value. When the *h_diff* value is larger, the intensity of the typhoon forecast is stronger and closer to the observation. Figure 2(a) shows that when the *h_diff* is small (*h_diff* value < 1.8 in IDE1, IDE2, IDE3, IDE4), the minimum sea surface pressure is maintained at about 1000 hPa during 60–78 h. The idealized experiment (IDE1, IDE2, IDE3, IDE4) results are quite different from those of IBTrACS, and the maximum difference reaches 70 hPa during 72–78 h. On the contrary, when *h_diff* is large (*h_diff* value$\geq$1.8 in IDE5 and IDE6), the forecasting effect of HWRF is significantly better. The minimum pressure of the idealized experiment forecast is smaller compared with IBTrACS over 60–66 h. After 66 h, the forecast error is almost 0 hPa. Compared with the other five experiments, the minimum pressure of IDE6 is closer to that of IBTrACS and its value reaches 930 hPa . Figure 2 (b) shows the relationship between the maximum wind speed and *h_diff* , which is similar to the minimum pressure in Fig. 2(a). The 10-m maximum wind speed difference between the idealized experiment (*h_diff* is small in IDE1–IDE4) and IBTrACS reaches 60 m/s. The 10-m maximum wind speed of the idealized experiment (*h_diff* is large in IDE5 and IDE6) is closer that of IBTrACS, and the maximum wind speed reaches 68 m/s. In summary, when *h_diff* is relatively large, the idealized experiment is closer to the observed result, and its forecast bias is significantly reduced.

Figure 3 shows the average forecast of the minimum pressure (a, c) and the maximum wind speed (b, d) over 60–78 h. It can be seen from Fig. 3(a) that the change in the minimum sea level pressure over 60–78 h is very sensitive to *h_diff*. When the *h_diff* is below 1.4, the minimum pressure value only reaches about 1000 hPa , but when *h_diff* is more than 1.4, the minimum pressure value changes suddenly, reaching below 940 hPa ; in particular, when *h_diff* is set to 2, the minimum pressure value is lower than 1.8. The same result was found for the maximum wind speed, as shown in Figs. 3(b) and 3(d). When *h_diff* reaches about 1.8, the maximum wind speed reaches 65 m/s, while at a smaller value of *h_diff* the maximum wind speed is only 20 m/s. Therefore, the greater the *h_diff*, the better the typhoon forecast.

To study the effect of *h_diff* on the typhoon structure and strength, the wind velocity profile with a radius of 150 km from the center of the typhoon is shown in Fig. 4. For the typhoon structure, the slope of the typhoon eye wall increases with *h_diff*. Clearly, when *h_diff* is 0.4 (IDE1), the slope of the typhoon eye wall is relatively inclined, and the 33 m/s wind profile reaches only 400 hPa. When the *h_diff* value reaches 1.4 (IDE4), the eye wall slope of the typhoon is closer to the vertical, and the 33 m/s wind profile reaches around 200 hPa. When *h_diff* is 2.0 (IDE6), it can be seen that the slope of the typhoon eye wall is the steepest, and the 33 m/s wind profile height is the highest at 150 hPa. Regarding the intensity of the typhoon, no matter how large the *h_diff* value is from 66 h to 69 h, the intensity of the typhoon is constantly increasing; plus, it can be seen that the red area is increasing, especially when *h_diff* is 2 (IDE6), and the maximum typhoon wind speed is obviously the strongest, which is the shape of a strong typhoon.

3.2 HWRF operational experiments with different PBL schemes

From the idealized experiment described above, when the horizontal diffusion coefficient *h_diff* is relatively large (*h_diff* $= 2$), the simulated strength is stronger and the structure is more symmetrical at the moment of explosive typhoon growth. Based on this result, four operational experiments (Table 2) were carried out and the results are described below.

Figure 5 shows the absolute bias of the typhoon intensity between the forecast and the best-track data (IBTrACS) for the four sensitivity experiments. Figure 5(a) shows the absolute bias from the typhoon occurrence to the development stage (0–60 h). It can be seen that the maximum bias of the four experiments does not exceed 10 hPa, indicating that the forecast from the typhoon

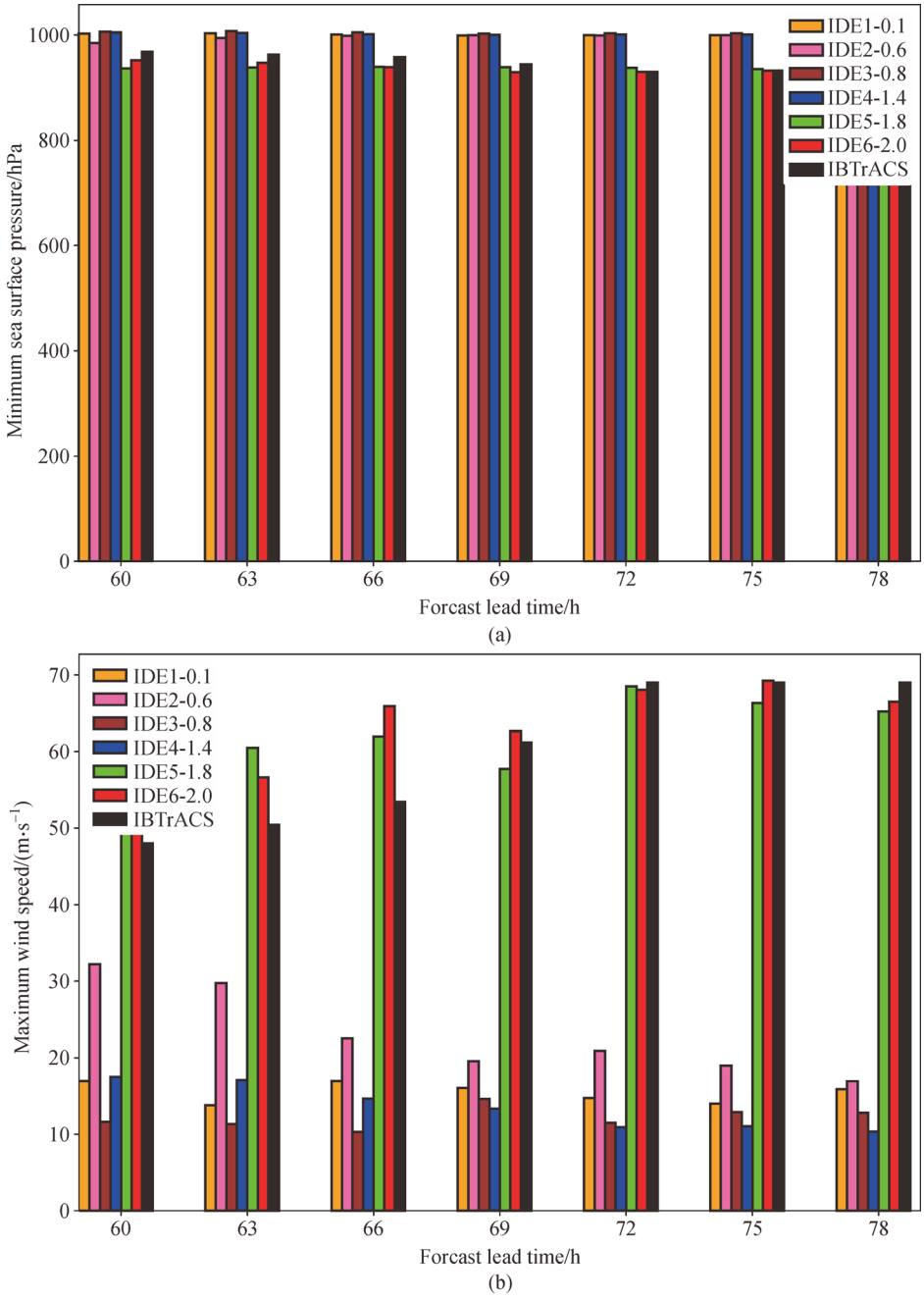

Fig. 2 (a) HWRF-ideal minimum sea surface pressure (hPa) and (b) maximum wind speed (m/s) over 60–78 h forecast. The *x*-axis is the effective time of the forecast, and the *y*-axis is the forecast intensity. The coloured histograms in the figure represent six ideal experiments, and the black histograms represent the results of IBTrACS.

occurrence to the development stage is a relatively better result, and the forecast biases of EXPR3 (solid green line) and EXPR4 (solid red line) are smallest, in which the maximum bias did not exceed 8 hPa. Compared with EXPR1 and EXPR2, when the horizontal diffusion coefficient is relatively small, the forecast bias is smaller. Figure 5(b) shows the forecast bias in the explosive growth stage of the typhoon, from which it can be seen that the forecast bias reaches its maximum at 69 h, and then gradually decreases. Compared with the same boundary layer parameterization scheme, after increasing the horizontal diffusion coefficient, the forecast bias is significantly reduced.

3.2.1 Contrast in the horizontal air–sea exchange coefficient

Bell et al. (2012) indicated that there is no significant change in the magnitude of the bulk exchange coefficients

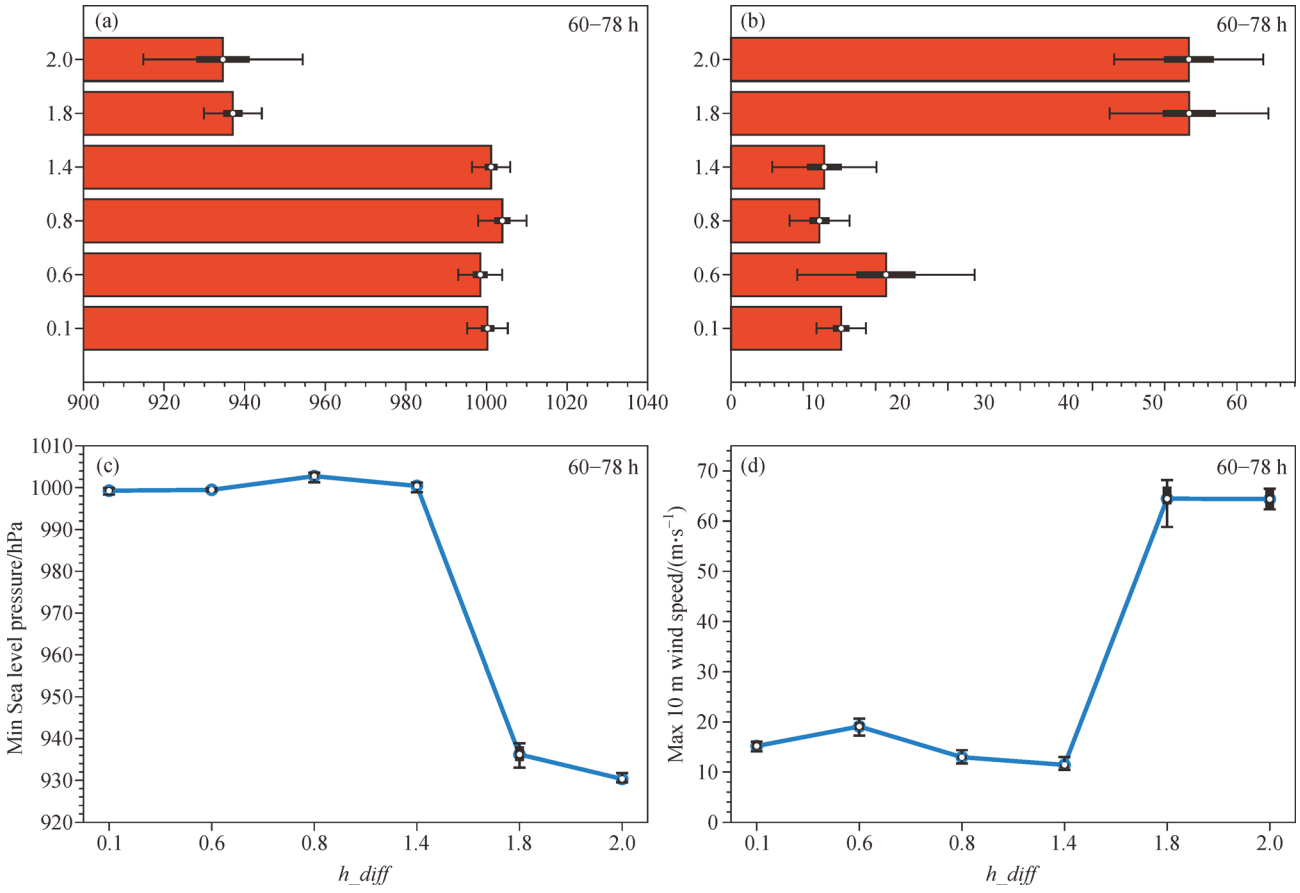

Fig. 3 Boxplot and Line-plot of HWRF-idealized 60–78h Mean Minimum Pressure (a), (c) and Mean Maximum Wind Speed (b), (d). The red bars in (a) and (b) represent Pressure and Wind speed, correspondingly. The blue lines in (c) and (d) also represent Pressure and Wind speed, correspondingly. The *x*-axis in (a) and (b) represents the Magnitude of Variable, and the *y*-axis represents *h_diff* values. The *x*-axis in (c) and (d) represents the *h_diff* value, and the *y*-axis represents the Magnitude of Variable.

estimated at minimal hurricane wind speeds, and that the ratio C_h/C_d does not significantly increase for wind speeds greater than 50 m/s. Therefore, we calculated the C_h/C_d output by HWRF to compare the simulation results of the four experiments.

The time series of C_h/C_d corresponding to the minimum pressure and maximum wind speed is plotted in Fig. 6. In general, during 0–78 h, the minimum pressure of the typhoon decreases and the maximum wind speed increases with the forecast lead time.

In EXPR1 (Figs. 6(a) and 6(e)), the minimum pressure can reach 974 hPa, corresponding to a C_h/C_d of about 1, and the maximum wind speed can reach 38 m/s , for which the corresponding C_h/C_d is 0.5. In EXPR3 (Fig. 6 (c) and 6(g)), the minimum pressure can reach 968 hPa, the corresponding C_h/C_d is within 0.5–1.25, and its maximum wind speed can reach 41 m/s, for which the corresponding C_h/C_d is 0.5, similar to EXPR1.

However, Figs. 6(c) and 6(g) show that, in EXPR3, the value of C_h/C_d is about 1.25–1.55, and the minimum pressure is also extremely reduced; the gradient of the slope (R = −1.3905) is steeper than for EXPR1 (R = −1.1642). At 66 h, the pressure reaches its lowest value of 966 hPa, and the maximum wind speed of the typhoon reaches 46 m/s, whose change is similar to that of the minimum pressure. Figures 6(d) and 6(h) show that the value of C_h/C_d in EXPR4 is the same as that in EXPR2, but its variance error is smaller and the change is more stable. The slope of the pressure in EXPR4 is the steepest among the four sensitivity experiments.

From the above analysis it can be seen that the value of C_h/C_d in EXPR2 and EXPR4 is obviously intensified compared with the results in EXPR1 and EXPR3; and in the experimental design, the former two experiments correspond to the QNSE boundary layer parameterization scheme, while the latter two correspond to the GFDL scheme. Therefore, the air–sea interface exchange coefficient has a significant influence on the simulated typhoon intensity of the different parameterization schemes. The larger the C_h/C_d, the stronger the intensity of the corresponding typhoon during the period of rapid intensification. The reason may be that, when C_h/C_d increases, the exchange flux at the air-sea interface increases, and the typhoon obtains more energy from the

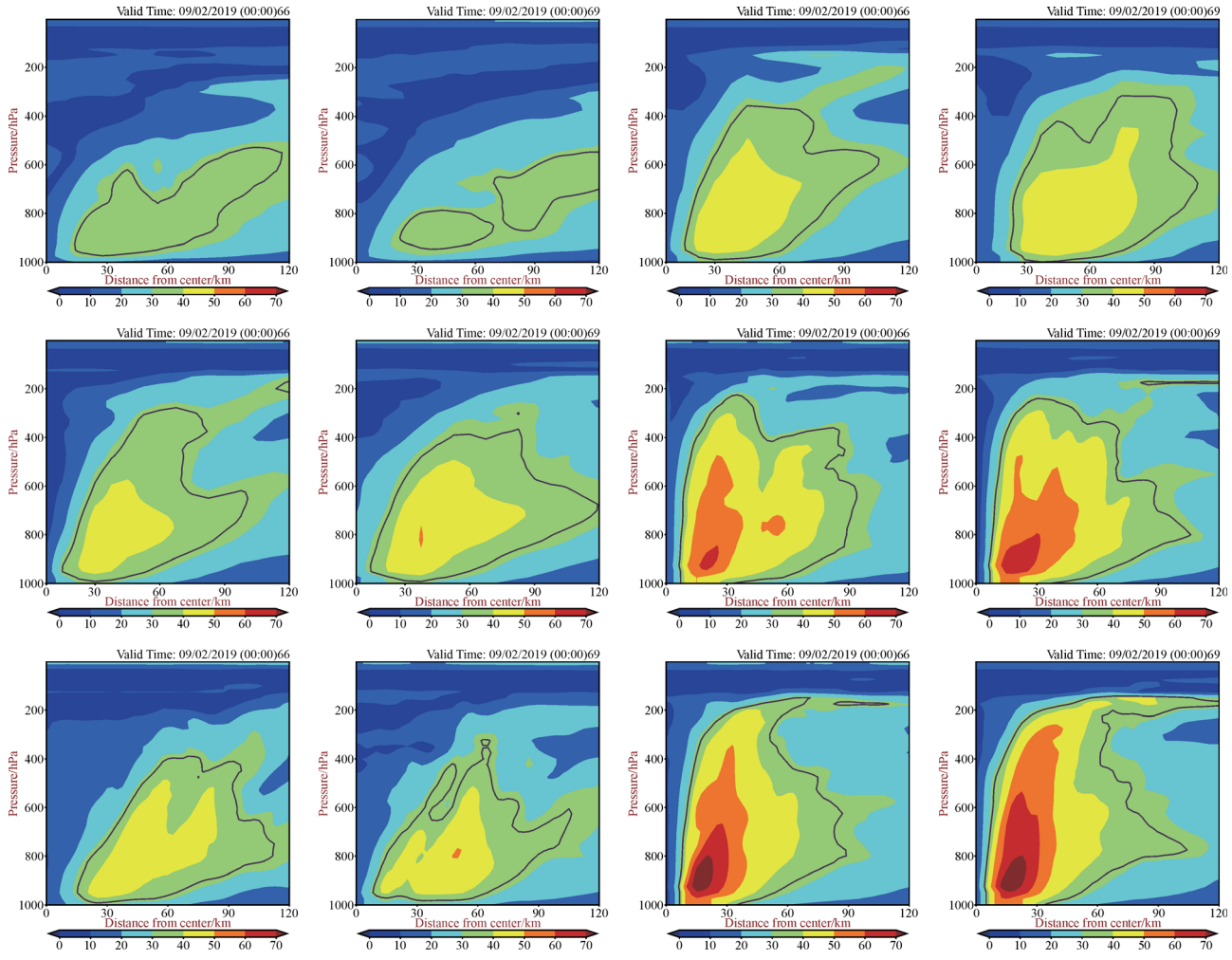

Fig. 4 Radius–height plots of the azimuthally tangential velocity at the (a) 66 h and (b) 69 h of the simulations for *h_diff* = (*IDE*1)0.4, (*IDE*2)0.6, (*IDE*3)0.8, (*IDE*4)1.4, (*IDE*5)1.8, (*IDE*6)2.0. The black contour has the value of 64 *kt* (33 m/s).

ocean, resulting in an increase in the intensity of the typhoon.

3.2.2 Typhoon cross sections

In order to further study the vertical structure of the typhoon, four groups of sensitivity experiments were selected for the forecasted wind speed field during 60–78 h, with the typhoon center as the center and the maximum wind speed radius as the radius tangent point to make a vertical section. Figure 7 shows a cross section of wind speed for the different boundary layer parameterizations and different horizontal diffusion coefficients (*h_diff*). The wind direction on both sides of the typhoon is obviously asymmetrical, with southerly wind on the northeast side and northerly wind on the southwest side during 60–78 h. With a time change to 60–72 h, the typhoon central structure shows quasi-symmetrical characteristics, and the height can reach about 200 hPa (Fig. 7, EXPR1). Moreover, the wind speed columns (large-value wind speed area) on both sides of the typhoon are also becoming more obvious. During 60–66 h, the low-level wind speed on the northeast side of the typhoon decreases from 48 m/s to 40 m/s; however, it increases from 40 m/s to 60 m/s at 72 h. The trend on the southwest side of the typhoon is similar to that on the northeast side, but the wind speed value is slightly smaller. However, at 78 h, the wind speed on the northeast side decreases and the height of the maximum value (wind speed > 40 m/s) is reduced to 600 hPa. The wind speed on the southwest side is weakened.

In EXPR3, during 60–66 h, the wind speed on both sides of the typhoon decreases from 48 m/s to 40 m/s on the northeast side and from 34 m/s to 28 m/s on the southwest side. Meanwhile, the cyclonic shear caused by the southerly wind and the northerly wind weakens. At 72 h, the wind speed on the southeast side of the typhoon reaches 60 m/s at the low level (below 700 hPa). The change on the southwest side is similar, and there are two large-value areas (wind speed > 40 m/s), with the wind

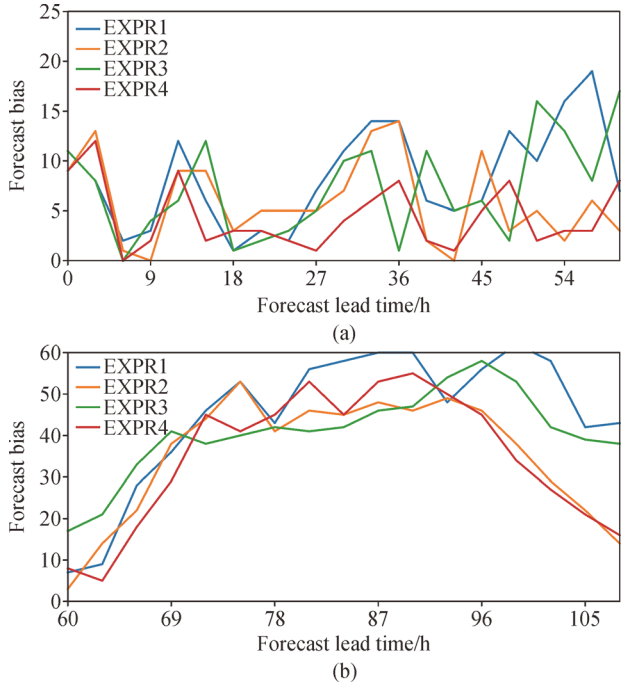

Fig. 5 The HWRF model forecast bias product with different planet boundary parameterization for "LINGLING". (a) is the absolute bias of intensity against IBTrACS over 0–54 h. The four coloured lines represent the four sensitivity experiments. [GFDL with *h_diff* = 1(EXPR1), QNSE(EXPR2), GFDL with *h_diff* = 2 (EXPR3), QNSE(EXPR4)].

speed increasing from 36 m/s to 40 m/s. On the contrary, the height of the large-value area on the northeast side decreases slightly. In general, the typhoon quasi-symmetrical structure in EXPR3 is more obvious than that in EXPR1 (Fig. 7). Comparing EXPR2 and EXPR4, it can be seen that the quasi-symmetrical structure in EXPR2 begins to disappear during 60–78 h; the low-level wind speed on the northeast side increases and the southerly wind strengthens, but both sides' wind speed column (red shaded part (> 48 m/s)) structures weaken during 60–66 h. At 72 h, the wind speed on both sides of the typhoon decreases, and the structure of the wind speed columns disappears. Below 700 hPa, the wind speed on the northeast side of the typhoon reaches 52 m/s , and a quasi-symmetrical structure appears at 78 h (EXPR4 in Fig. 7). It can be seen that, during 60–78 h, the quasi-symmetrical structure begins to weaken with time and the large wind speed area on both sides is reduced. However, the quasi-symmetrical structure of the typhoon still exists compared with EXPR2. From the low level to the high level, the wind provides water vapor and energy for the development of the typhoon.

Based on the above analysis of wind speed, the four experiments show that, during the period of 60–78 h, the changes on both sides of the typhoon center are not very large, and wind speed shows alternating positive and negative changes. Meanwhile, the adjustment has a positive impact on the typhoon intensity forecast, making

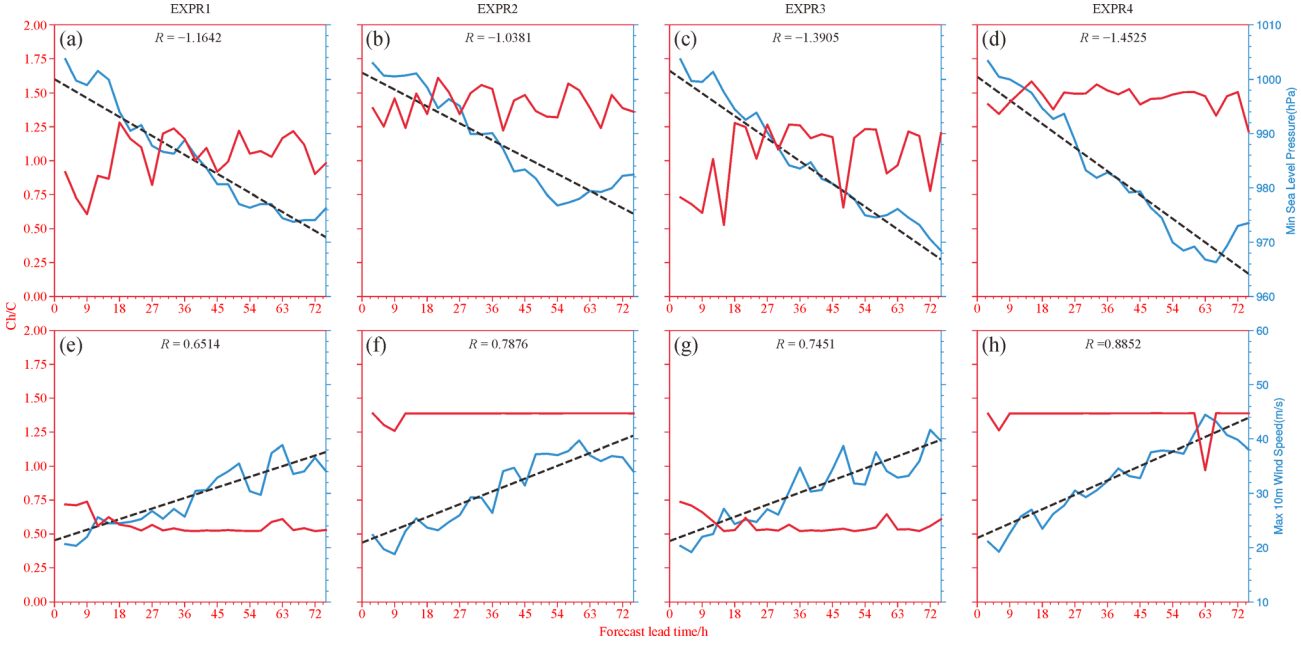

Fig. 6 Forecast 78 h Line Chart Plot of Different Boundary Layer Parameterization schemes with different *h_diff* of HWRF correspond to the Minimum Pressure, the Maximum wind speed and its corresponding C_h/C_d.The *x*-axis represents of Forecast Lead Hours, the *y*1-axis (Left) represents of the value of C_h/C_d, the *y*2-axis (Right) represents of the value of Min Sea Level Pressure (hPa) and Max 10 m Wind Speed (m/s). The black dashed line in the figure represents the slope of minimum pressure and maximum wind speed. Slope is *R*.

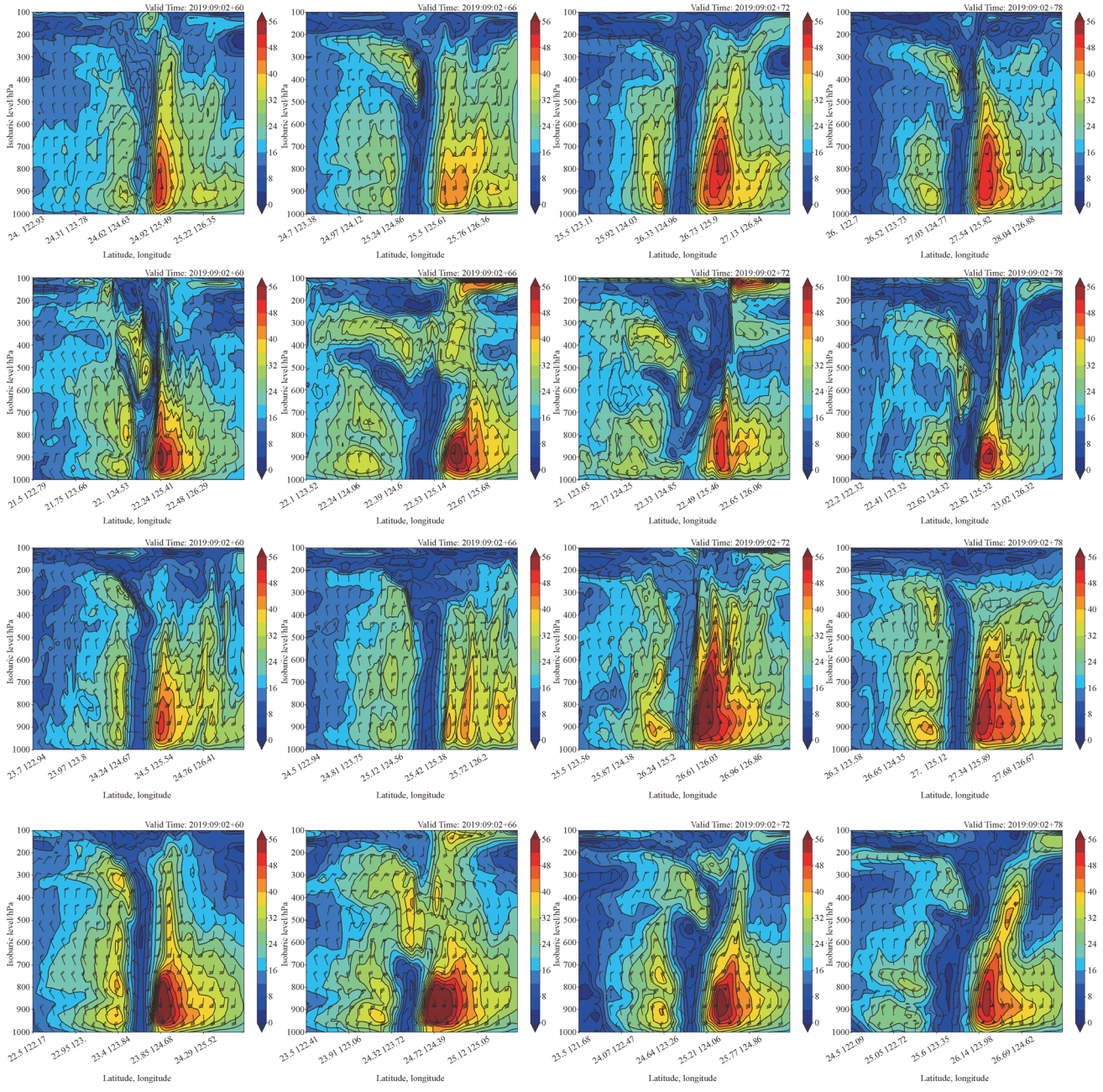

Fig. 7 The wind-speed cross-section of HWRF model using different planetary boundary layer parameterization at 60 to 78 h. The four rows relatively as EXPR1, EXPR2, EXPR3, EXPR4. The *x*-axis represents the cross location of latitude/longitude, and *y*-axis represents isobaric level (hPa). The wind arrows represent radial wind speed and tangential wind speed of the cross-section profile.

it closer to the observations. In addition, the greater the value of *h_diff*, the greater the contribution to the structure of the typhoon during the period of rapid intensification.

3.2.3 Wind profile comparison with MEERA2

Figures 8(a), 8(b) and 8(c), 8(d) show the vertical profile of the averaged radial and tangential wind speed at the radius of maximum wind (RMW) and 2 × RMW, respectively, during 54–69 h. It can be seen that the trends of the radial and tangential wind profiles of EXPR1 and EXPR3 are consistent with those of MERR2, but are not within the range of MERR2's standard deviation of one. However, the wind profiles of EXPR2 and EXPR4 possess large variations, showing opposite trends in the upper and lower levels (Fig. 8(a)). The maximum radial wind speed appears between 860 and 950 hPa, while above 800 hPa the wind speed decreases and the rate of change with height is small.

The maximum radial wind speed of EXPR4 (QNSE, *h_diff* = 2) is 30 m/s, and the maximum radial wind speed of EXPR1 (GFDL, *h_diff* = 1) is the smallest compared with the other three experiments (Fig. 8(b)). It can be seen that the wind speeds of the four experiments show an increasing–decreasing trend with height. Below 850 hPa, the largest increase in tangential wind speed is in EXPR2, which can reach 48 m/s; the smallest increase in tangential wind is in EXPR1. This result corresponds to the previous maximum wind speed and minimum air pressure changes. When *h_diff* is increased, the simulation result of the typhoon in HWRF is closer to the actual measurement. In

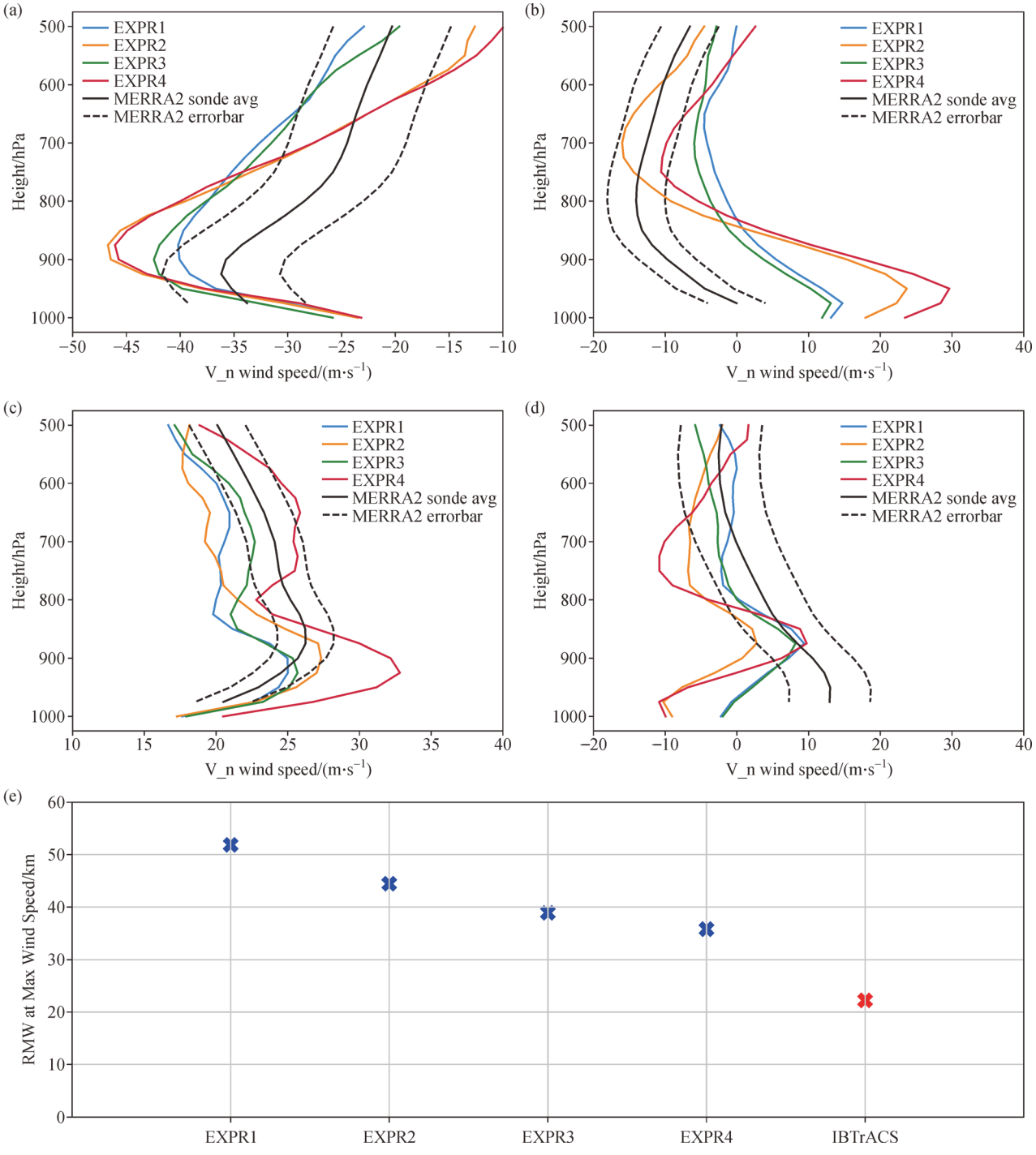

Fig. 8 The average radial and tangential wind profiles of the four HWRF sensitivity experiments during the 60–78 h forecast. (a) and (b) represent at RMW, (c) and (d) represent at 2RMW, and the colored solid lines represent four sensitivity experiment groups respectively, the black experiment represents the MERRA2 result, and the black dotted line represents the result of 1 standard deviation. (e) Refers to the point map of the average maximum wind speed radius of the four groups of experiments in the typhoon forecast 60–78 h.

the radial wind speed at 2 × RMW (Fig. 8(d)), MERRA2 first decreases with height and then increases in the opposite direction, but the wind speed at the upper layers is almost 0 m/s. The corresponding results of the four HWRF sensitivity experiments have opposite changes at the lower level, which show a process of turning a negative wind speed value to a positive value. As a whole, it can be seen that both EXPR1 and EXPR3 are within one standard error of MERRA2. After the *h_diff* is increased, the range of the maximum wind speed corresponding to EXPR2 and EXPR4 falling within the interval of one standard deviation increases significantly (Fig. 8(c)). It can be seen that the simulation results corresponding to EXPR3 and EXPR4 are similar to those of MERRA2, falling within the range of one standard deviation of the observations, and reaching more than 80%.

In conclusion, it was found that, around the eye wall of the typhoon, the vertical change of wind speed in the lower level is greater than that in the upper level, which is related to the interaction between the typhoon and the sea. Following the dynamical argument of Kilroy et al. (2016), more horizontal diffusion yields stronger radial pressure gradients and stronger inflow in the boundary layer. With stronger inflow, contraction of the storm is favored.

3.2.4 Budget analyses of the absolute angular momentum

Budget analyses of the absolute angular momentum ($M = rV_r + 2fr^2$, where r is radial distance and f is the Coriolis parameter) were performed to elucidate the mechanisms that might contribute to intensity and structure change. The budget equation of the azimuthally averaged M tendency is given by

$$\frac{\partial\langle M\rangle}{\partial t} = -\langle V_r\rangle\frac{\partial\langle M\rangle}{\partial r} - \langle w\rangle\frac{\partial\langle M\rangle}{\partial z} - \langle V_r'\frac{\partial M'}{\partial r}\rangle - \langle w'\frac{\partial M'}{\partial z}\rangle + F_r, \tag{13}$$

where w is the vertical velocity. The brackets denote an azimuthal average at constant height, and the primes denote a departure from the azimuthal mean (or eddy). Note that all velocities in Eq. (13) are storm relative. The terms on the right-hand side of Eq. (13) are, respectively, the mean radial advection of $\langle M\rangle$, the mean vertical advection of $\langle M\rangle$, the radial advection of the resolvable eddy angular momentum, the vertical advection of the resolvable eddy angular momentum, and the combined diffusive and boundary layer tendency (F_r). (The term F_r is the combination of the vertical and horizontal diffusion caused by subgrid processes). To investigate the role of *h_diff* in modulating the gain/loss of M, the total mean advection of M and the sum of the eddy terms were calculated and compared with the tendency of M and the F_r term.

Figure 9 shows time averages of the terms in the azimuthally averaged angular momentum of Eq. (13) during the period of rapid intensification (between 60 and 78 h). In the four experiments, the total average convection of $\langle M\rangle$ and the F_r term are the main factors for the gains and losses of $\langle M\rangle$, and the changes of these two items are roughly the same in the typhoon structure, but the signs are opposite. Therefore, the overall change trend of $\langle M\rangle$ is relatively gentle. As expected, when increasing the horizontal diffusion coefficient, the negative F_r term decreases accordingly . The spin-up of the vortex in the boundary layer is mainly due to the positive mean advection of $\langle M\rangle$, which is mainly from the horizontal mean advection component or the convergence of $\langle M\rangle$. The convergence of $\langle M\rangle$ exceeds the boundary layer friction and diffusion caused by subgrid processes, which is the same as the result reported by Zhang and Marks (2015).

Comparing the same boundary layer parameterization scheme, it can be seen from EXPR1 and EXPR3 that when increasing the horizontal diffusion, the $\frac{\partial\langle M\rangle}{\partial t}$ of EXPR3 is on the whole comparable with EXPR1 when obtaining the angular momentum during the explosive growth stage of the typhoon, and, correspondingly , the advection term increases and the F_r decreases, meaning the intensity of the typhoon increases. It can be seen from EXPR2 and EXPR4 that the same conclusions can be reached. When increasing the horizontal diffusion coefficient, the time-varying term of $\langle M\rangle$ increases and the range of increase in the advection term is smaller than that of the F_r. Overall, the typhoon tends to become stronger. This result indicates the important role of *h_diff* in regulating the relative contributions to the total tendency of M from the resolved and unresolved eddies.

3.2.5 Horizontal and vertical diffusion eddies

Horizontal and vertical diffusion eddies are not directly output by the model. The calculation of horizontal vortex diffusion is based on Eqs. (7) and (8). For the calculation method of vertical diffusion eddies, Tang et al. (2018b) used the fast-response wind data collected by a multi-level tower to calculate the vertical vortex diffusion using two different methods (direct flux theory and thermodynamic theory), and Ma et al. (2018) used the Yonsei University (YSU) scheme, which is a nonlocal closure scheme using the *K*-profile approach to represent vertical mixing within the boundary layer. In this paper, the calculation of vertical diffusion eddies was calculated based on the *K*-profile, but differed from the YSU calculation method and was similar to the thermodynamic method of Tang et al. (2018a); namely, Eq. (4).

The horizontal diffusion eddy, as a function of the mean wind speed for each run, is shown in Fig. 10, indicating an increasing trend of it with the wind speed up to the maximum wind speed. Figure 10(e) shows the function of

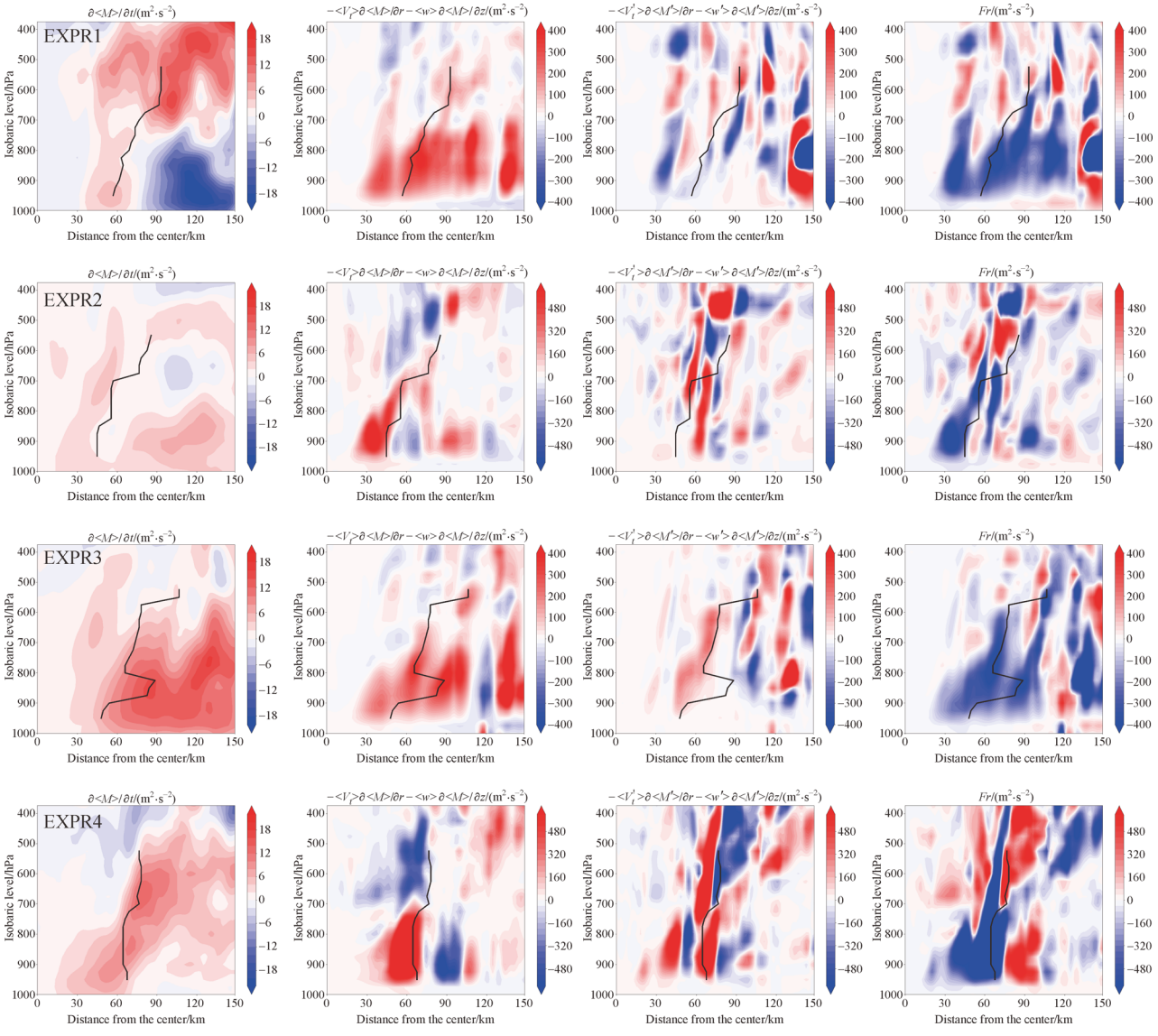

Fig. 9 Radius–height plots of the terms in the azimuthally averaged absolute angular momentum (M) budget for simulations with the four HWRF sensitivity experiments during the forecast over 60–78 h. EXPR1, EXPR3, EXPR2, and EXPR4 are the prediction results. The x-axis represents the distance from the typhoon center, and y-axis represents the isobaric level. The black line represents the radius of maximum azimuthally averaged tangential wind speed.

the horizontal diffusion eddy and horizontal wind speed calculated from ERA5 data. It can be seen that there is a direct positive correlation between horizontal wind speed and diffusion. Comparing the same boundary layer parameterization scheme, from EXPR1 and EXPR3 it can be seen that when increasing the horizontal diffusion coefficient, the fit between horizontal vortex diffusion and horizontal wind speed is closer to a positive correlation, similar to the result with ERA5. The same conclusion can be drawn from EXPR2 and EXPR4.

Figure 11 shows the vertical eddy diffusivity as a function of height. From the experiment with the GFDL boundary layer parameterization scheme, it can be seen that the vertical diffusion eddy reaches its maximum at 500 m as the height increases. When the height continues to increase, the vertical diffusion eddy shows a decreasing trend, which is similar to the findings of Zhang et al. (2020). When increasing the horizontal diffusion coefficient, the vertical diffusion eddy simulated by EXPR3 is greater than the vertical vortex diffusion simulated by EXPR1. Therefore, for the GFDL parameterization scheme, after increasing the horizontal diffusion coefficient, the corresponding horizontal diffusion eddy and vertical diffusion eddy are increased, so the typhoon intensity increases. Similar results were found for the QNSE parameterization scheme. The difference from the GFDL scheme is the relationship between the vertical diffusion eddy and height. It can be seen from EXPR2 and

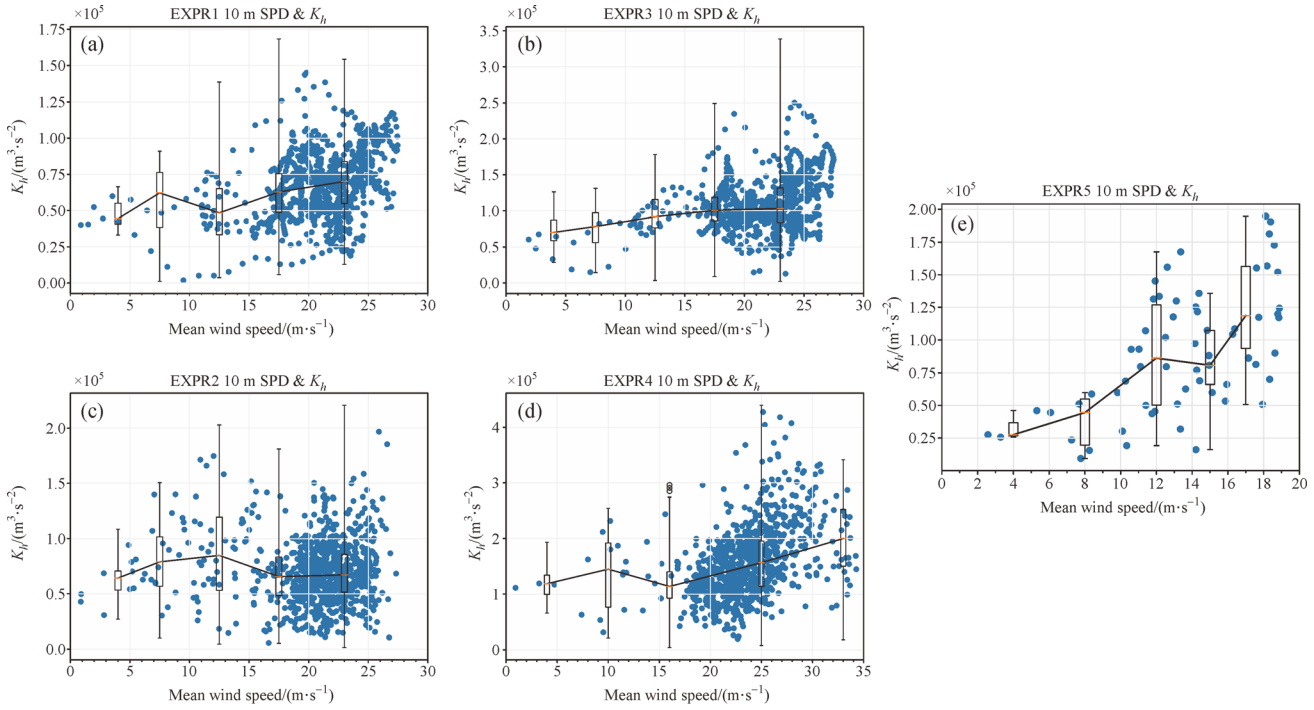

Fig. 10 Horizontal diffusion eddy as a function of wind speed at surface of the four HWRF sensitivity experiments during the forecast over 60–78 h. (a) EXPR1, (b) EXPR3, (c) EXPR2, and (d) EXPR4 are the prediction results. (e) Represents the result calculated by ERA5. The *x*-axis represents the mean wind speed (m/s) ,and *y*-axis represents the horizontal diffusion eddy (m^3/s^2).

EXPR4 that the vertical diffusion eddy has been increasing as the height increases. This is because the height of the boundary layer fitted by the QNSE parameterization scheme is 10 orders of magnitude larger than that of the GFDL scheme. Figure 12 shows the horizontal diffusion eddy (K_m) as a function of the vertical diffusivity eddy (K_h) at the surface of the four HWRF sensitivity experiments during the forecast period of 60–78 h. It can be seen that horizontal mixing and vertical mixing are more sensitive to the horizontal diffusion coefficient. Comparing EXPR1 and EXPR3, it can be seen that when we increase the horizontal diffusion coefficient, the maximum value of horizontal mixing increases to 2.7×10^5 m^3/s^2 ; plus, the large-value range of vertical mixing is also larger than that of EXPR1, and the maximum value can reach almost 3×10^3 m^2/s^2 . The same conclusion can also be reached from EXPR2 and EXPR4. Comparing different boundary layer parameterization schemes, it can be seen that the vertical mixing corresponding to the QSNE scheme is significantly stronger than that of the GFDL scheme. In short, when we increase the horizontal diffusion coefficient, the corresponding horizontal and vertical diffusion eddies increase correspondingly, so the typhoon intensity increases.

3.2.6 Ocean feedback to typhoon precipitation

Ma et al. (2020) combined satellite observations to reveal that the cold wakes left by TCs effectively regulate local cloud cover and rainfall. When a TC moves slowly or is strong, clouds and rainfall tend to be more suppressed. In warmer climates, this modulation can be amplified as the strength of the TC's movement increases or decreases. Therefore, starting from the ocean feedback, we discuss whether the results of the four sets of experiments reported in this paper reflect the above conclusions for the simulation of typhoon precipitation. Figure 13 depicts the simulation of typhoon clouds and rain during the explosive growth stage of the typhoon in this study. By comparing EXPR1 and EXPR2, it can be seen that the range and intensity of QNSE precipitation is much smaller than that of GFDL. At the same time, comparing the typhoon positions fitted by the two schemes, the movement speed of the QNSE typhoon is obviously slower than the typhoon fitted by GFDL. From 66 to 72 h, the position of GFDL has moved from the central part of the Taiwan Peninsula to its north, while the typhoon fitted by QNSE shows movement from the southern part of the Taiwan Peninsula. When we increase the horizontal diffusion coefficient, comparing EXPR3 and EXPR4, this conclusion becomes more obvious. Therefore, the conclusion of Ma et al. (2020) can be confirmed insofar as that when the intensity of the typhoon increases or the speed of movement slows down, the amount of precipitation and cloud cover in the typhoon-cooled wake area decreases.

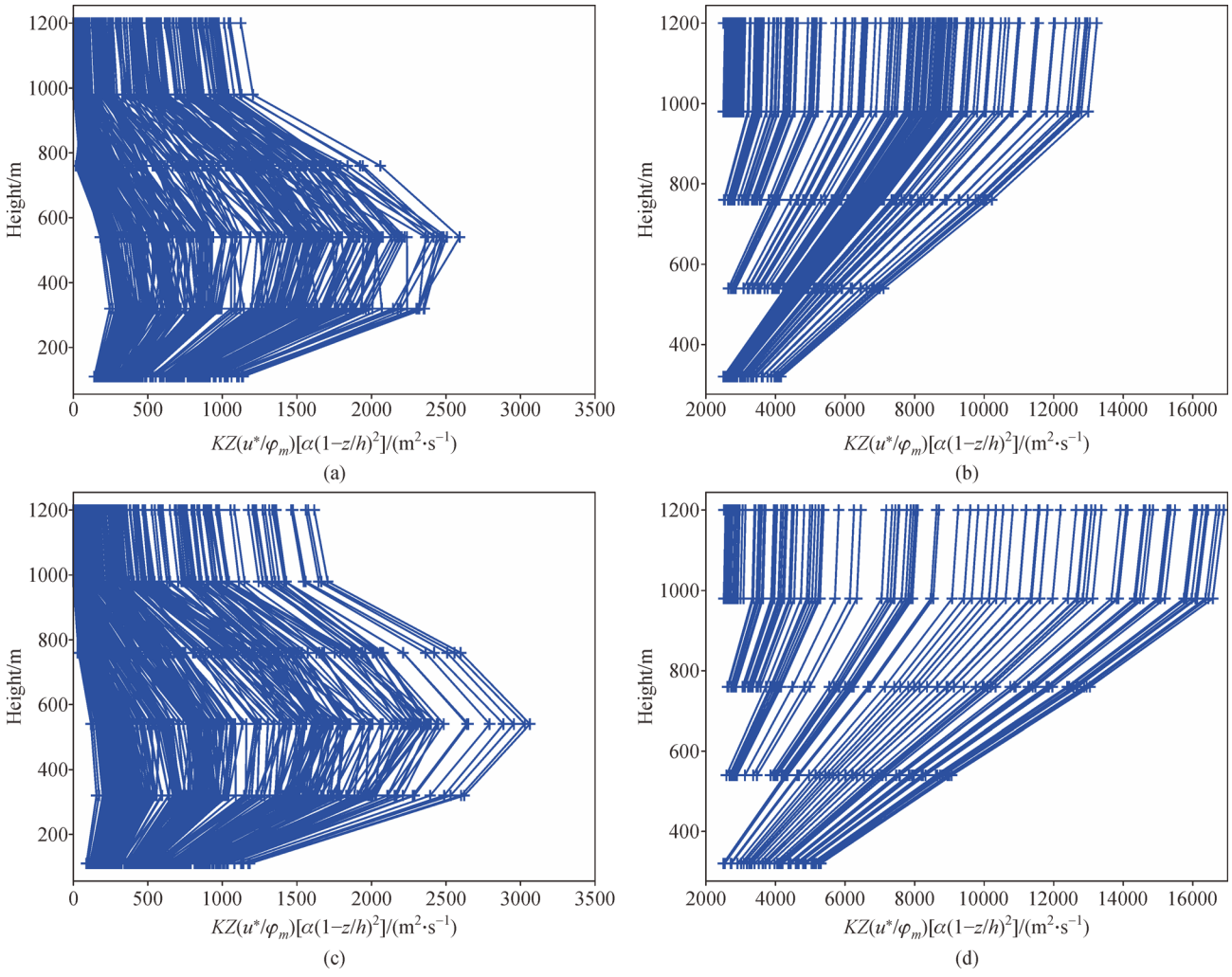

Fig. 11 Vertical eddy diffusivity (K_m) as a function of height for the four HWRF sensitivity experiments during the forecast over 60–78 h. EXPR1, EXPR2, EXPR3, and EXPR4 represents (a), (b), (c) and (d). The *x*-axis represents the Vertical eddy diffusivity (K_m) (m^2/s^2),

4 Discussion and conclusions

With the development of numerical weather prediction models, typhoon track forecasts have been significantly improved, but typhoon intensity forecasts remain challenging (Xue et al., 2013), especially for explosive typhoons. The forecast uncertainty is closely associated with the choice of boundary layer parameterization scheme. Meanwhile, many researchers have paid attention to the influence of the horizontal diffusion coefficient of the air–sea interface on the forecasting of typhoon intensity. Zhang and Marks (2015) pointed out that the horizontal mixing length (L_h) is highly sensitive to the structure and intensity of the typhoon. Based on the sensitivity of PBL parameterization and horizontal diffusion, we designed six idealized experiments to simulate the occurrence and development of the 15th typhoon that occurred in the western Pacific in 2019 — namely, typhoon Lingling.

The idealized experiment was used to explore the effect on typhoon prediction by modifying the horizontal diffusion coefficient (*h_diff*). From the results, we have been able to draw the following preliminary conclusions: The larger the horizontal diffusion coefficient is, the stronger the simulated typhoon intensity will be, which is closer to the IBTrACS best-track observations. When *h_diff* is set to 2, the corresponding minimum pressure and maximum wind speed can reach 930 hPa and 65 m/s. It can be seen from the cross section of the typhoon wind speed that the larger the *h_diff* value, the better the structure of the simulated typhoon intensity, and a steeper slope can be obtained in the simulated typhoon eye area.

Based on the conclusion of the idealized experiment, we designed four operational experiments by using two different PBL parameterization schemes with two different horizontal diffusion coefficients. The results showed that the four experiments were able to simulate the intensity well in the typhoon development stage, with the bias all within 10 hPa. However, there was no explosive growth

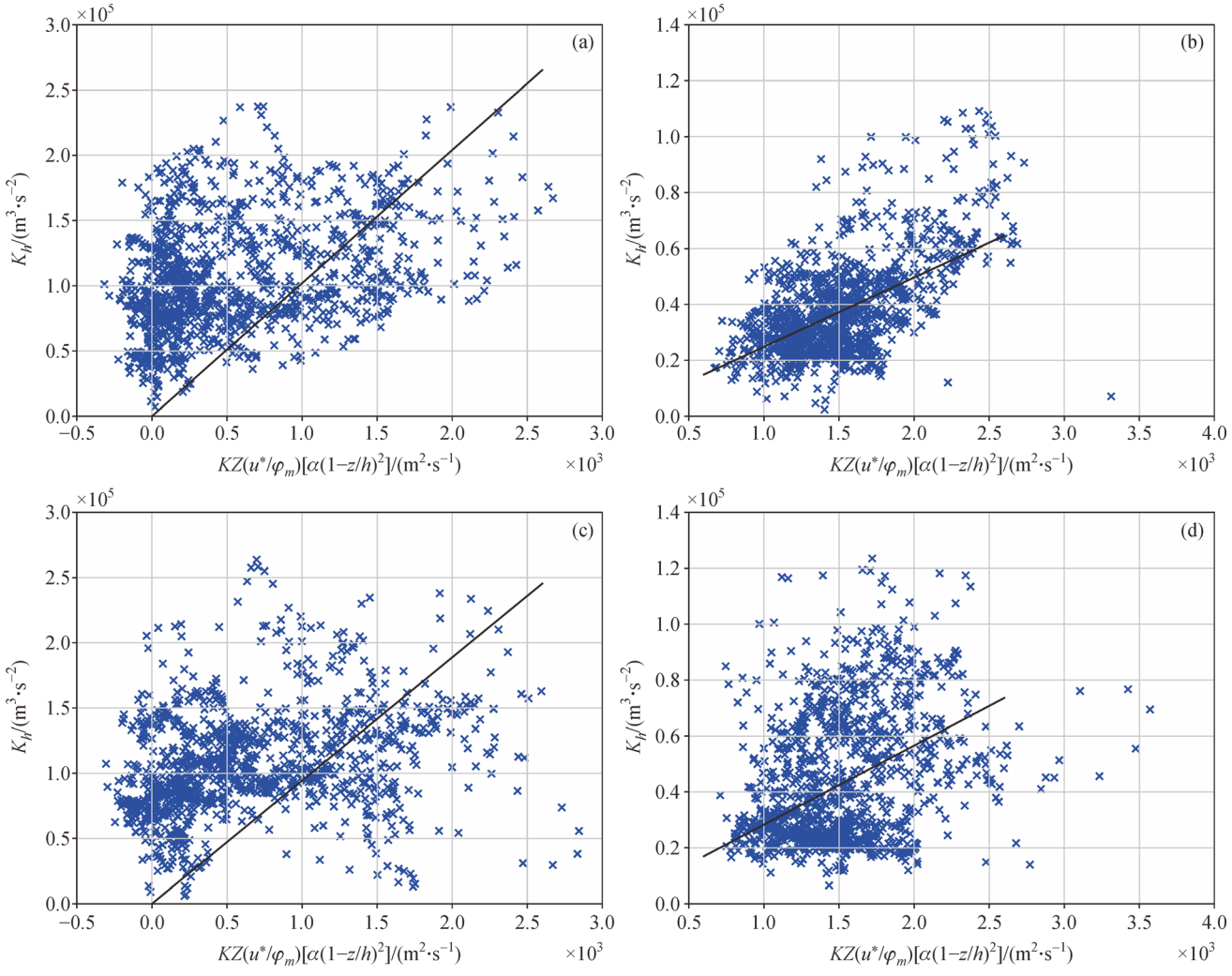

Fig. 12 Horizontal diffusion eddy as a function of Vertical eddy diffusivity at surface of the four HWRF sensitivity experiments during the forecast over 60–78 h. EXPR1 (a), EXPR2 (b), EXPR3 (c), and EXPR4 (d) are the prediction results. The *x*-axis represents the Vertical eddy diffusivity (K_m) (m^2/s^2), and *y*-axis represents the horizontal diffusion eddy (K_h) (m^3/s^2).

predicted after 60 h (development of the typhoon), and so this was further studied. Forecast verifications (Fig. 5) showed that when using the same parameterization scheme in EXPR3 and EXPR4 ($h\_diff = 2$), the prediction skill of HWRF model was higher than that of EXPR1 and EXPR2 ($h\_diff = 1$). However, the forecast bias increased significantly after 66 h. From the four sensitivity experiments (Fig. 5(b)), it was found that the forecast bias of EXPR2 was the largest and EXPR3 the smallest. The forecast bias for the QNSE boundary layer parameterization scheme had a larger simulation bias of typhoon intensity than the GFDL simulation during the explosive growth stage, but the bias gradually decreased after 69 h, which shows the hysteresis in intensity simulation. When the horizontal diffusion coefficient (*h_diff*) was large, regardless of the PBL parameterization scheme, the forecast bias was smaller than that when *h_diff* was small. To study why the QNSE scheme possesses better simulation strength than the GFDL scheme, the role of air–sea exchange was analyzed. The neutral drag coefficient controlling the momentum exchange is C_d, and the coefficient controlling the heat exchange at the air–sea interface is C_h. Emanuel (1986) pointed out the maximum hurricane wind speed has long been hypothesized to be proportional to $\left(\frac{C_h}{C_d}\right)^{1/2}$. According to Fig. 6, the higher the C_h/C_d, the higher the wind speed predicted by HWRF, and the faster the rate of change in the maximum wind speed and minimum pressure. The value of the air–sea interface exchange coefficient of the QNSE scheme is obviously greater than the exchange coefficient in the GFDL scheme. When $\frac{C_h}{C_d}$ is larger, the exchange flux at the air-sea interface

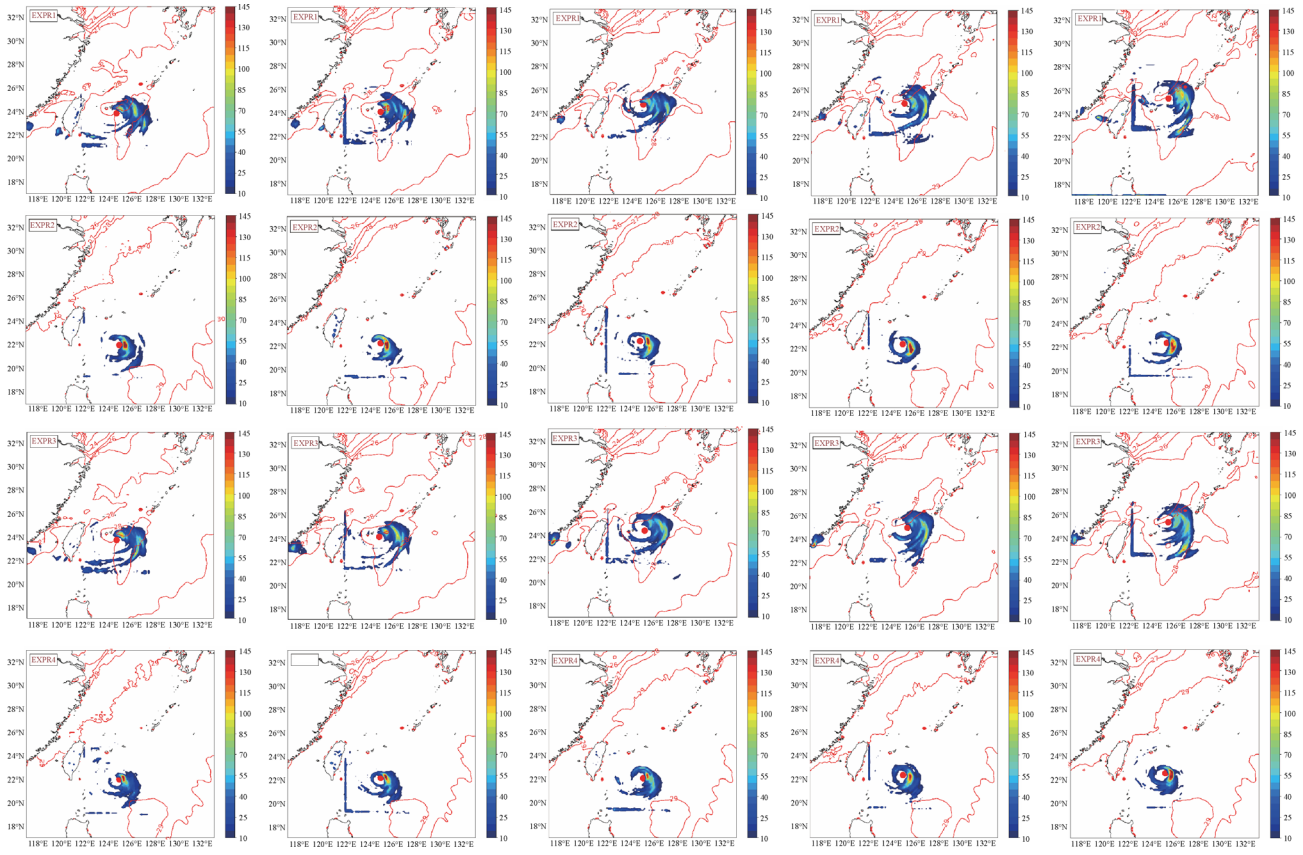

Fig. 13 Four sets of sensitivity experiments correspond to the 3 h accumulative precipitation for typhoon forecast 60–78 h. The red dot in the picture represents the typhoon center.

increases, and the typhoon obtains more energy from the ocean, resulting in an increase in the intensity of the typhoon.

Next, we analyzed the changes in the vertical structure of the typhoon during the explosive growth phase. Taking the typhoon center as the coordinate center, we took vertical sections of the four runs of the typhoon during 54–78 h. Based on the analysis of wind speed, the four experiments showed that, during the period of 60–78 h, the changes on both sides of the typhoon center were not very large, and wind speed had alternating positive and negative changes. Meanwhile, the adjustment had a positive impact on the typhoon intensity forecast, making it closer to the observations. In addition, the greater the value of *h_diff*, the greater the contribution to the structure of the typhoon in the explosive stage.

During the period of rapid intensification, when the horizontal diffusion coefficient was stronger, the corresponding typhoon simulation intensity was stronger and the wind speed of the boundary layer was larger. The stronger wind speed inflow, plus the larger radial gradient of angular momentum, made the convergence of the angular momentum larger, enhancing the typhoon intensity. Angular momentum budget analyses indicated that, when increasing the *h_diff*, the time-varying term of angular momentum M increases, and the range of increase in the advection term was smaller than the range of F_r. The convergence of angular momentum was larger in the boundary layer, which led to a faster spin-up of the vortex, further increasing the intensity of the typhoon.

It is noticeable that many researchers have calculated and analyzed the horizontal and vertical vortex diffusion. Therefore, the horizontal and vertical vortex diffusion of the four sets of experiments were calculated according to Eqs. (4), (7), and (8). When the *h_diff* was increased, the corresponding wind speed and horizontal vortex diffusion relationship was closer to the observation, and the corresponding horizontal vortex diffusion also showed an increasing trend. In the vertical vortex diffusion, meanwhile, when the *h_diff* was increased, the corresponding vertical vortex diffusion also increased, which further confirms that the F_r term in M was increasing in Fig. 9, and the typhoon M increased during the explosive growth stage, resulting in a stronger simulation of the typhoon intensity. Ma et al. (2020) concluded that, as the intensity of a typhoon increases or the speed of movement slows down, precipitation and cloud cover in the typhoon-cooled wake area decrease. On this basis, we analyzed the corresponding typhoon precipitation during the explosive growth stage (54–78 h), from which it was found that the

typhoon intensity corresponding to the QNSE scheme was stronger than that of the GFDL scheme; plus, the typhoon's speed of movement simulated by the QNSE scheme was slower than that of the GFDL scheme. It was revealed that the typhoon precipitation corresponding to the QNSE scheme was significantly weaker than that of the GFDL scheme, thus verifying the conclusion of Ma et al. (2020).

This study was based on the simulation of a single apidly intensifying typhoon in its initial stage in the western Pacific basin in 2019. The bias of the HWRF forecast is still large. In future research, typhoon simulations in the western Pacific will continue to be studied based on data assimilation and model boundary layer parameterization. Due to the lack of data, the assimilation used by HWRF is only 3DVAR (three-dimensional variational), and the ocean model used is POM, which may produce different results for late typhoon prediction owing to the different dynamic and heat exchange in different ocean models during air–sea coupling. We will continue to focus on the effects of air–sea coupled momentum, heat exchange coefficients, and assimilation of sensitive areas in typhoon prediction. Zhang et al. (2016) pointed out that the ensemble transform method can be useful in providing guidance for adaptive observation deployment. Therefore, this method will be used to further study the assimilation of sensitive areas in typhoon observations.

Acknowledgements This study was jointly supported by the Guangdong Basic and Applied Basic Science Research Foundation (No. 2019B1515-120018), a project of Enhancing School with Innovation of Guangdong Ocean University (No. 230419053), projects (platforms) for Construction of Top-ranking Disciplines of Guangdong Ocean University (No. 231419022), and the Special Funds of Central Finance Support of the Development of Local Colleges and Universities (No. 000041).

References

Bell M M, Montgomery M T, Emanuel K A (2012). Air–sea enthalpy and momentum exchange at major hurricane wind speeds observed during CBLAST. J Atmospheric Sci, 69: 3197–3222

Biswas M K, Coauthors (2018). 2018: Hurricane Weather Research and Forecasting (HWRF) Model: 2018. Scientific Documentation

Braun S A, Tao W K (2000). Sensitivity of high-resolution simulations of Hurricane Bob (1991) to planetary boundary layer parameterizations. Mon Weather Rev, 128(12): 3941–3961

Bryan G H (2012). Effects of surface exchange coefficients and turbulence length scales on the intensity and structure of numerically simulated hurricanes. Mon Weather Rev, 140(4): 1125–1143

National Centers for Environmental Prediction/National Weather Service/NOAA/U.S. Department of Commerce (2015). NCEP GFS 0.25 Degree Global Forecast Grids Historical Archive

Emanuel K A (1995). Sensitivity of tropical cyclones to surface exchange coefficients and a revised steady-state model incorporating eye dynamics. J Atmos Sci, 52(22): 3969–3976

Emanuel K A (1997). Some aspects of hurricane inner-core dynamics and energetics. J Atmos Sci, 54(8): 1014–1026

Emanuel K A (1986). An air–sea interaction theory for tropical cyclones. Part I: steady-state maintenance. J Atmos Sci, 43(6): 585–605

Gelaro R, McCarty W, Suárez M J, Todling R, Molod A, Takacs L, Randles C, Darmenov A, Bosilovich M G, Reichle R, Wargan K, Coy L, Cullather R, Draper C, Akella S, Buchard V, Conaty A, da Silva A, Gu W, Kim G K, Koster R, Lucchesi R, Merkova D, Nielsen J E, Partyka G, Pawson S, Putman W, Rienecker M, Schubert S D, Sienkiewicz M, Zhao B (2017). The modern-era retrospective analysis for research and applications, Version 2 (MERRA-2). J Clim, 30(14): 5419–5454

Gray W M, Ruprecht E, Phelps R (1975). Relative humidity in tropical weather systems. Mon Weather Rev, 103(8): 685–690

Green B W, Zhang F (2014). Sensitivity of tropical cyclone simulations to parametric uncertainties in air–sea fluxes and implications for parameter estimation. Mon Weather Rev, 142(6): 2290–2308

Hariprasad K B R R, Srinivas C V, Singh A B, Vijaya Bhaskara Rao S, Baskaran R, Venkatraman B (2014). Numerical simulation and intercomparison of boundary layer structure with different PBL schemes in WRF using experimental observations at a tropical site. Atmos Res, 145–146: 27–44

Janjić Z I (1990). The step-mountain coordinate: physical package. Mon Weather Rev, 118(7): 1429–1443

Kilroy G, Smith R K, Montgomery M T (2016). Why do model tropical cyclones grow progressively in size and decay in intensity after reaching maturity? J Atmos Sci, 73(2): 487–503

Knapp K R, Kruk M C, Levinson D H, Diamond H J, Neumann C J (2010). The international best track archive for climate stewardship (IBTrACS). Bull Am Meteorol Soc, 91(3): 363–376

Ma Z, Fei J, Huang X, Cheng X (2018). Sensitivity of the simulated tropical cyclone intensification to the boundary-layer height based on a K-profile boundary-layer parameterization scheme. J Adv Model Earth Syst, 10(11): 2912–2932

Ma Z, Fei J, Lin Y, Huang X (2020).Modulation of clouds and rainfall by tropical cyclone's cold wakes. Geophys Res Lett, 47: e2020GL-088873

Malkus J S, Riehl H (1960). On the dynamics and energy transformations in steady-state hurricanes. Tellus, 12(1): 1–20

Nolan D S, Stern D P, Zhang J A (2009). Evaluation of planetary boundary layer parameterizations in tropical cyclones by comparison of in situ observations and high-resolution simulations of hurricane Isabel (2003). Part II: inner-core boundary layer and eyewall structure. Mon Weather Rev, 137(11): 3675–3698

Ooyama K (1969). Numerical simulation of the life cycle of tropical cyclones. J Atmos Sci, 26(1): 3–40

Persing J, Montgomery M T (2003). Hurricane superintensity. J Atmos Sci, 60(19): 2349–2371

Rajeswari J R, Srinivas C V, Rao T N, Venkatraman B (2020). Impact of land surface physics on the simulation of boundary layer characteristics at a tropical coastal station. Atmospheric Res, 238: 104888

Rosenthal S L (1971). The response of a tropical cyclone model to variations in boundary layer parameters, initial conditions, lateral boundary conditions, and domain size. Mon Weather Rev, 99(10): 767–777

Rotunno R, Bryan G H (2012). Effects of parameterized diffusion on simulated hurricanes. J Atmos Sci, 69(7): 2284–2299

Rotunno R, Chen Y, Wang W, Davis C, Dudhia J, Holland G J (2009). Large-eddy simulation of an idealized tropical cyclone. Bull Am Meteorol Soc, 90(12): 1783–1788

Smith R K, Montgomery M T, Van Sang N(2009). Tropical cyclone spin-up revisited. Q J R Meteorol Soc, 135(642): 1321–1335

Stevens B, Moeng C H, Sullivan P P (1999). Large-eddy simulations of radiatively driven convection: sensitivities to the representation of small scales. J Atmos Sci, 56(23): 3963–3984

Tang J, Zhang J A, Aberson S D, Marks F D, Lei X (2018a). Multilevel tower observations of vertical eddy diffusivity and mixing length in the tropical cyclone boundary layer during landfalls. J Atmos Sci, 75 (9): 3159–3168

Tang J, Zhang J A, Kieu C, Marks F D (2018b). Sensitivity of hurricane intensity and structure to two types of planetary boundary layer parameterization schemes in idealized HWRF simulations. Trop Cyclone Res Rev, 7: 201–211

Wang Y (1995). An inverse balance equation in sigma coordinates for model initialization. Mon Weather Rev, 123(2): 482–488

Xue M, Schleif J, Kong F, Thomas K W, Wang Y, Zhu K (2013). Track and intensity forecasting of hurricanes: impact of convection-permitting resolution and global ensemble Kalman filter analysis on 2010 Atlantic season forecasts. Weather Forecast, 28(6): 1366–1384

Zhang J A, Montgomery M T (2012). Observational estimates of the horizontal eddy diffusivity and mixing length in the low-level region of intense hurricanes. J Atmos Sci, 69(4): 1306–1316

Zhang J A, Uhlhorn E W (2012). Hurricane sea surface inflow angle and an observation-based parametric model. Mon Weather Rev, 140(11): 3587–3605

Zhang J A, Marks F D (2015). Effects of horizontal diffusion on tropical cyclone intensity change and structure in idealized three-dimensional numerical simulations. Mon Weather Rev, 143(10): 3981–3995

Zhang J A, Marks F D, Sippel J A, Rogers R F, Zhang X, Gopalakrishnan S G, Zhang Z, Tallapragada V (2018). Evaluating the impact of improvement in the horizontal diffusion parameterization on hurricane prediction in the operational hurricane weather research and forecast (HWRF) Model. Weather Forecast, 33(1): 317–329

Zhang J A, Kalina E A, Biswas M K, Rogers R F, Zhu P, Marks F D (2020). A review and evaluation of planetary boundary layer parameterizations in hurricane weather research and forecasting model using idealized simulations and observations. Atmosphere, 11 (10): 1091

Zhang Y, Xie Y, Wang H, Chen D, Toth Z (2016). Ensemble transform sensitivity method for adaptive observations. Adv Atmos Sci, 33(1): 10–20